HHS Public Access

Author manuscript

ACS Appl Bio Mater. Author manuscript; available in PMC 2021 June 25.

Published in final edited form as:

ACS Appl Bio Mater. 2020 October 19; 3(10): 7147–7157. doi:10.1021/acsabm.0c00949.

Combination of Disulfiram and Copper–Cysteamine Nanoparticles for an Enhanced Antitumor Effect on Esophageal Cancer

Yan Chang[#a], **Fang Wu**[#a,b], **Nil Kanatha Pandey**[#c], **Lalit Chudal**[c], **Meiying Xing**[c], **Xiaoli Zhang**[d], **Linh Nguyen**[e], **Xian Liu**[f], **J. Ping Liu**[c], **Wei Chen**[c,*], **Zui Pan**[a,*]

[a]College of Nursing and Health Innovation, The University of Texas at Arlington, TX, 76019, USA;

[b]Department of Radiation Oncology, First Affiliated Hospital of Guangxi Medical University, Nanning, Guangxi, 530021, P. R. China;

[c]Department of Physics, The University of Texas at Arlington; Arlington, TX 76019, USA;

[d]Center for Biostatistics, The Ohio State University Medical Center, Columbus, OH, 43210, USA;

[e]Department of Biology, The University of Texas at Arlington; Arlington, TX 76019, USA;

[f]Department of Kinesiology, College of Nursing and Health Innovation, The University of Texas at Arlington, TX, 76019, USA.

[#] These authors contributed equally to this work.

Abstract

Esophageal cancer (EC) is the sixth leading cause of cancer deaths worldwide with a low 5-year survival rate. More effective chemotherapeutic drugs, either new or repurposing ones, are urgently needed. Disulfiram (DSF) is a safe and public domain drug for alcohol addiction treatment and later shown to have anti-cancer capability, especially when administrated together with copper. The present study is to test the hypothesis that a newly developed copper-cysteamine (Cu-Cy) nanoparticles (NPs) can enhance the anti-tumor effect of DSF on esophageal cancer with reduced risk of copper poisoning. Our results showed that Cu-Cy NPs could greatly facilitate DSF to inhibit cell proliferation in cultured human esophageal cancer cells. Interestingly, the combined inhibitory function could be further enhanced when DSF and Cu-Cy NPs were present at an optimal molar ratio of 1:4. The results of the change in physical color, UV-vis absorption and fluorescence spectra, X-ray diffraction patterns, and FTIR spectra from a mixture of DSF and Cu-Cy NPs suggest a possible reaction between DSF and Cu-Cy NPs and the formation of new materials. Furthermore, cellular mechanistic studies revealed that the combination of DSF and Cu-Cy NPs resulted in reactive oxygen species (ROS) accumulation, and blocked nuclear translocation of NF-ƙB (p65) in esophageal cancer cells. Moreover, in xenograft nude mice, combined administration of DSF and Cu-Cy NPs greatly inhibited tumor growth without

[*]**Corresponding Author:** To whom correspondence should be addressed: Zui Pan, zui.pan@uta.edu; Wei Chen, wei.chen@uta.edu.

Author Contributions

Conceptualization: ZP, WC, YC, FW, NKP; Methodology and analysis: YC, FW, NKP, LC, MX, XZ, LN, XL, JPL; Writing: ZP, WC, YC, NKP, LC.

There are no conflicts to declare.

noticeable histological toxicity, while any single agent at the same doses presented no inhibitory function. Together, this study demonstrates an effective anti-cancer function of combined treatment of DSF and Cu-Cy NPs in vitro and in vivo, which could be a promising new chemotherapy for esophageal cancer patients.

Keywords

Apoptosis; proliferation; reactive oxygen species (ROS); NF-κB; esophageal squamous cell carcinoma

INTRODUCTION

As a leading cause of cancer deaths worldwide, esophageal cancer (EC) contains two main types, i.e. esophageal adenocarcinoma and esophageal squamous cell carcinoma (ESCC). Both types are often diagnosed at a late stage and become unsuitable for surgery management. More effective chemotherapeutic agents for EC patients are required[1].

Disulfiram (tetraethylthiuram disulfide, DSF), also known by its trade name Antabuse which has been approved by the Food and Drug Administration (FDA) to treat alcoholism for over 60 years[2–3]. The mechanism of anti-alcohol activity is to inhibit aldehyde dehydrogenase (ALDH), an enzyme that converts acetaldehyde to acetate. The rapidly increased concentration of acetaldehyde in the blood after drinking causes unpleasant body reactions, such as facial flush, headache, and vomiting, thereby deterring alcohol consumption[3–5]. Due to its mild toxicity and manageable adverse effects, DSF has been attracting research interests to be repurposed in the treatment of other diseases. In recent years, DSF has been found effective against a wide variety of cancer types in preclinical studies and emerged as a promising repurposed chemotherapeutic drug[2–3, 6]. In addition to inhibiting ALDH, other mechanisms of action of DSF exist, such as inducing reactive oxygen species (ROS) accumulation, regulating nuclear factor-κB (NF-κB) and/or ERK signaling pathways, and inhibiting drug-resistant involved ATP-binding cassette (ABC) transporters[7]. All these mechanisms of action contribute to its anti-tumor or reversing drug resistance functions. The anti-tumor effect of DSF can be greatly enhanced by the addition of copper (Cu). It is, in part, attributed to that DSF is able to chelate tumor intracellular Cu, resulting in binding to and inhibition of the proteasome and in turn initiating cancer cell apoptosis[2, 6, 8]. Other mechanisms underlying the enhanced anti-tumor effect of DSF by Cu may exist as well. Despite accumulating evidence from preclinical studies to show the effectiveness of DSF in the treatment of a wide range of cancers, clinical trials using DSF either alone or together with Cu as chemotherapy, haven’t been able to demonstrate the same result. Some trials were terminated due to a lack of clear beneficial outcomes at the tolerable dosage range[7]. It is of importance to develop a strategy to enhance the anti-tumor efficacy of DSF/Cu for its successful clinical translation.

During the progression of cancer, elevated Cu concentrations in serum and tumor tissues have been observed[7, 9]. The elevated Cu concentration in tumor tissues appears to be insufficient to work together with DSF to carry out their anti-cancer effects. Therefore, the oral administration of Cu gluconate has been included in DSF clinical trials. Since Cu is a

heavy metal with significant toxicity to normal cells, the safe dosage window for Cu is limited. To improve the biodistribution of Cu to tumor tissues, Cu-based nanoparticles (NPs) become to be an attractive option because NPs can accumulate in tumor tissue via enhanced permeability and retention (EPR) effect[10].

Copper-cysteamine (Cu-Cy) NP is a newly developed nanoparticle which can produce ROS under UV light[11], X-ray[12–15], microwave[11, 16] or ultrasound for cancer treatment[17–19]. Furthermore, these NPs can be utilized to destroy bacterial cells under UV light. A recent report further demonstrated that Cu-Cy NPs act as a Fenton-like catalyst for cancer cell destruction with high selectivity in the presence of endogenous hydrogen peroxide[20]. This present study provided evidence to show that Cu-Cy NPs can provide Cu ions to active DSF in cancer cells and thus achieve a greatly enhanced anti-tumor effect in EC. Since Cu-Cy NPs are able to accumulated in the tumor tissues via EPR effects, data further showed that combined Cu-Cy NPs with DSF could have an effective anti-tumor function with reduced toxicity in normal cells *in vivo*.

MATERIAL AND METHODS

Materials.

Copper chloride dihydrate ($CuCl_2.2H_2O$), cysteamine hydrochloride, sodium hydroxide (NaOH), polyethylene glycol 4000, dihydrorhodamine 123 (DHR), dihydroethidium (DHE) and coumarin were bought from Sigma-Aldrich, USA. All the chemicals were used as received.

Synthesis of Cu-Cy NPs.

Cu-Cy NPs were fabricated by following our previously published method[11]. Typically, copper chloride dihydrate (273 mg) was mixed into DI water (50 mL) and stirred vigorously under ambient temperature. Cysteamine hydrochloride (381 mg) and polyethylene glycol 4000 (40 mg) were subsequently added into the mixture under a nitrogen atmosphere. After pH adjusting to 7, the nitrogen environment was removed and the reaction mixture was stirred for about 5 min until the color turned to deep violet. The reaction mixture was then heated (100 °C) for 5 min under the nitrogen environment. After allowing the solution to cool naturally, the product was centrifuged and washed with a mixture of ethanol and water three times. The Cu-Cy particles were obtained after drying in a vacuum oven at 40 °C. The detailed characterizations and crystal structure of Cu-Cy NPs were described in previous publications[11, 21].

Fluorescence and UV-Vis Absorption Spectroscopy.

The photoluminescence (PL) spectra of Cu-Cy+DSF (DSF:Cu-Cy=1:4) suspended in ethanol after 4 h of incubation was taken by a spectrofluorophotometer (Shimadzu RF-5301PC). For the purpose of comparison, the PL spectra of Cu-Cy NPs alone was measured at two different time points (0 and 4 h) under identical experimental conditions. The UV-Vis absorption spectra of different molar ratios of DSF to Cu-Cy (DSF:Cu-Cy=50:1, 10:1, 1:1,1:4, and 1:8) dispersed in ethanol were recorded after 4 h of incubation

using a spectrophotometer (Shimadzu UV-2450). Also, the absorption spectra of different concentrations of DSF alone or Cu-Cy NPs alone were measured as well.

X-ray Diffraction (XRD) Patterns.

Powder XRD patterns were taken using a Rigaku Ultima IV diffractometer with Cu K_α radiation (λ = 0.15406 nm). Samples containing various molar ratios of DSF to Cu-Cy (10:1, 1:1,1:4, and 1:8) were prepared in ethanol. After 4h of incubation, the samples were deposited on glass substrates and allowed to dry at room temperature. XRD spectra of DSF alone or Cu-Cy alone were carried out under the same experimental conditions.

Fourier-Transform Infrared (FTIR) Spectroscopy.

In order to measure the FTIR spectrum of Cu-Cy+DSF combination, DSF and Cu-Cy were mixed in ethanol at the molar ratio of 1:4 (DSF:Cu-Cy=1:4). After 4 h of incubation, the supernatant was removed by centrifugation and subsequently washed 1 time with ethanol and dried in a vacuum. The FTIR spectrum of the powder sample was then carried out using a FTIR spectrometer (Shimadzu IRPrestige/PIKE MIRacle). The control experiments were performed by taking Cu-Cy powder only and DSF powder only under the same instrumental conditions.

ROS Detection Using Fluorescent Probes.

ROS generated by Cu-Cy+DSF (DSF:Cu-Cy=1:4) in cell-free solution was examined by the photoluminescence (PL) method utilizing DHR as a ROS probing agent[22]. The stock solutions of DHR (1.54 mM) and DSF (6 mM) were made in dimethylformamide (DMF). Subsequently, a working solution (final volume 3 mL) containing DHR (12.83 μM), Cu-Cy NPs (200 μM), DSF (50 μM), and H_2O_2 (100 μM) was prepared in a cuvette (10 mm path length). The PL intensity was measured by the spectrofluorophotometer at 524 nm with 1.5 nm slits after different incubation periods with the excitation wavelength at 495 nm. The control experiments were carried out by taking DI water only, H_2O_2 only, DSF+H_2O_2, or Cu-Cy+H_2O_2 under the same experimental conditions.

Intracellular ROS was detected by monitoring the PL of DHE. KYSE-30 cells were seeded in the black clear bottom 96-well plate at the confluency of 80% and incubated in dark for 30 min at 37 °C, 5% CO_2 once after adding 5 μM DHE. After removing the old medium with DHE, cells were treated with 4 μM Cu-Cy, 1 μM DSF, 4 μM Cu-Cy and 1 μM DSF combination, 12 μM $CuCl_2$ and 1 μM DSF combination, 12 μM $CuCl_2$ in the medium without phenol red for 1h, 2h, 3h and 4h separately. The fluorescent signal was measured at 480 nm excitation and 570 nm emission on microplate reader SpectraMax® i3 (Molecular Devices, CA).

Hydroxyl Radical (•OH) Detection in a Cell-free System.

•OH generated by Cu-Cy+DSF (DSF:Cu-Cy=1:4) in aqueous solution in the presence of H_2O_2 (100 μM) was measured by the PL method using coumarin as described previously with slight modifications[11]. Briefly, the required amount of DSF and Cu-Cy were separately added to 50 mL of DI water followed by 30 min of sonication. Then, a 3 mL of testing solution in DI water (10 mm path length cuvette) was made by mixing coumarin (0.1 mM),

Cu-Cy (200 μM), DSF (50 μM), and H_2O_2 (100 μM). Afterward, the PL intensity was recorded at 452 nm by the spectrofluorophotometer at various incubation periods with the excitation wavelength of 332 nm. The control experiments were performed by taking DI water alone, H_2O_2 alone, DSF+H_2O_2 or Cu-Cy+H_2O_2 under the same experimental conditions.

Cell Culture.

Human ESCC cells (KYSE-30) were cultured as described previously[1, 23]. In brief, ESCC cells were maintained in the medium comprising 47% RPMI-1640 and 47% Ham's F12 medium (Corning, US), 5% fetal bovine serum (FBS, VWR, US) and 1% penicillin/ streptomycin (Corning, US). The culture condition was maintained at 37 °C, 5% CO_2 with humidity.

MTT Assay.

ESCC cells were seeded in 200 μL cell culture medium per well into the 96-well plate and incubated with different concentrations of DSF, Cu-Cy, or $CuCl_2$ either alone or in combination for 48 h or 72 h. Then, 5 mg/mL 3-(4, 5-dimethylthiazol-2-yl)-2, 5-diphenyl-tetrazolium bromide (MTT) was added into cell culture medium and incubated with cells at 37 °C in dark for 3 h. After removal of the cell culture medium, DMSO (100 μL/well) was employed to dissolve the formazan. Lastly, absorbance was recorded at 570 nm on microplate reader SpectraMax® i3 (Molecular Devices, CA). The relative cell viability and IC_{50} calculation were conducted by using Graphpad Prism 5 (San Diego, US).

NF-κB/p65 Nuclear Translocation Assay.

KYSE-30 cells were seeded on the glass bottom dish at the confluency of 80%. After serum starvation for 2 h, cellular growth was stimulated by the addition of 10% FBS in culture medium. Cu-Cy NPs (4 μM), DSF (1 μM), or their combination were added in cell culture medium at indicated timepoint. After fixation in 4% paraformaldehyde buffer, cells were permeabilized in PBS with Triton X-100 (0.1%) followed by blocking with goat serum (10%) solution for 1 h. After washing with PBS, cells were treated with primary antibody anti-NF-κB/p65 (1:50, Santa Cruz, US) and incubated overnight at 4 °C, followed by incubation of their second antibodies, i.e. goat anti-rabbit IgG labelled with Alexa 488 (Abcam, US). Nuclei were stained by cell membrane permeable dye Hochest 33342 (Enzo, US). The specific signals for each fluorescent probes were captured by DMi8 inverted fluorescent microscope equipped with Hamamatsu digital camera C11440 and 40x objective (NA 1.3, Leica, Germany).

Xenograft Tumor Growth Assay.

Animal protocol was approved by the Institutional Animal Care and Utilization Committee (IACUC) at the University of Texas at Arlington. Male NCr nu/nu nude mice were purchased from Jackson Lab at 6 to 7 week old. KYSE-30 cells (1×10^6) in 100 μL PBS were added with the same volume of matrigel (Corning, US) and sebsequently subcutaneously inoculated into the back of each mouse. Tumors became to be visible and reached ~ 5 mm diameter one week after inoculation. Then all mice were randomly divided into 4 groups:

DSF (1 μM), Cu-Cy (4 μM), Cu-Cy + DSF (4 μM, 1 μM, respectively), $CuCl_2$ + DSF (12 μM, 1 μM, respectively). All compounds were administrated daily by i.p injection, and the amounts were calculated according to the body weight of that day. body weights and tumor volumes were measured every two days. Tumor volume (mm^3) was determined using the equation: Volume = 3.14/6 × length × $(width)^2$. At the end of the experiment, all mice were euthanized and tumor and all key organs for each animal were gathered.

H&E Staining.

Tumor tissues, kidney, heart, liver, spleen and lung were immediately fixed in 10% neutral buffered formalin overnight. After paraffin embedding, deparaffinization and rehydration, 5 μm longitudinal sections were stained with hematoxylin solution staining for 3 min followed by incubation in in 1% HCL-ethanol (1% HCl in 70% ethanol) for 10 s. The sections were rinsed with distilled water, stained with eosin solution for 10 min, and then dehydrated and cleared in xylene. Finally, the sections were mounted with neutral balsam and monitored under an inverted microscope (DMi8) supplied with color camera 2900 and 20x objective (NA 0.35, Leica, Germany).

Statistical Analysis.

Prism 5 (GraphPad, San Diego, CA) was used for statistical analyses. Data are presented as the mean ± standard error of the mean (S.E.M). Significant differences were considered significant at a P value < 0.05 in all cases. In animal experiments, each group contains 6 mice, and a linear mixed effects model was used in the statistical analysis of tumor growth. It took account of the correlation among observations from the same animal. The tumor volume was first transformed by log2 to reduce variance and skewness. The significant difference was shown between the groups.

RESULTS

Combination of DSF and Cu-Cy NPs Inhibited Cell Proliferation in KYSE-30 Cells.

To examine the combination of DSF and Cu-Cy NPs on cell viability in KYSE-30 cells, we first tested the dose-dependent curves of the individual components using MTT assay (Figure 1A–B). DSF could inhibit cell proliferation in KYSE-30 cells in a dose-dependent manner with IC_{50} at 68.0 μM (Figure 1A). Consistent with previous reports, Cu-Cy NPs were able to induce cell death and reduce cell viability at room light, even though much less efficient than UV or X-ray (Figure 1B)[12]. Then, we tested the inhibitory effect of combination of DSF and Cu-Cy NPs at concentrations 50 μM and 1 μM, respectively. The statistical analysis of cell viability demonstrated that combination of DSF (50 μM) and Cu-Cy NPs (1 μM) achieved a significantly better inhibitory effect than any single agent alone (Figure 1C). Interestingly, with the equal amount of Cu-Cy NPs at 1 μM, DSF concentration at 1 μM could induce more cell death in KYSE-30 cells (15% vs. 33% of cell viability) (Figure 1D). Data suggest that the anti-cancer effect of DSF and Cu-Cy NPs may be dependent upon the formation of new complex material at a certain ratio rather than simple additive effects.

Effect of DSF on Physical Color and Luminescence of Cu-Cy NPs.

In order to observe the physical color of different combinations of DSF and Cu-Cy NPs, stock solutions of DSF and Cu-Cy NPs were prepared in ethanol and DI water, respectively. After that, various ratios of DSF to Cu-Cy were prepared diluting in DI water. It is showed that the different ratios of DSF to Cu-Cy (50:1, 10:1, 1:1, 1:4, and 1:8) and Cu-Cy alone after 4 h of incubation under room light (top) and UV light (bottom) (Figure 2A). As shown in Figure 2A (top), Cu-Cy NPs presented clear color under room light. With increasing ratio and concentration of DSF, the color turned into brown, indicating a possible reaction between DSF and Cu-Cy NPs and subsequent formation of a DSF-copper complex[8, 24]. Consistent with the changes in color under room light, the bright orange fluorescent color of the Cu-Cy NPs upon UV light (365 nm) decreased gradually with the increase in DSFconcentration. When the ratio of DSF to Cu-Cy reached to 50:1, Cu-Cy NPs completely lost its luminescence within 4 h of incubation.

Next, the PL spectra of Cu-Cy NPs dispersed in ethanol were compared with or without DSF after 4 h of incubation (Figure 2B). The PL intensity of Cu-Cy+DSF (DSF:Cu-Cy=1:4) was noticeably reduced when compared to Cu-Cy alone. As DSF has the ability to react with thiol groups[8, 25], the reduction in the PL intensity of Cu-Cy+DSF is most likely due to the breaking of the thiol group of Cu-Cy by DSF, thereby resulting in the formation of a DSF-Cu complex. It should be worthwhile mentioning that the PL intensity of Cu-Cy at 0 and 4 h did not change noticeably, signifying the stability of Cu-Cy NPs.

UV-Vis Absorption Spectra of Various Molar Ratios of DSF to Cu-Cy.

In order to identify the end product from the reaction of DSF and Cu-Cy NPs, UV-Vis absorbance spectroscopy was adopted. The disappearance of the characteristic peak of Cu-Cy at 365 nm suggested that the chemical reaction has occurred between DSF and Cu-Cy (Figure 2C). Moreover, a strong peak at about 433 nm was observed in all combinations of Cu-Cy and DSF (DSF:Cu-Cy=50:1, 10:1, 1:1, 1:4, and 1:8) but absent in Cu-Cy or DSF alone (Figure 2D), indicating that a chemical reaction between Cu-Cy and DSF may result in the formation of copper diethyldithiocarbamate ($Cu(DDC)_2$) complex[26–31]. Furthermore, the peaks observed at 270 and 290 nm in the UV region (Figure 2C) are ascribed to the π-π^* transition of S — C — N and S — C —S chromophores, respectively[31]. The stronger signals revealed more $Cu(DDC)_2$ production with a higher ratio of DSF. The UV-vis absorbance spectra (Figure 2C–D) and physical color change along with the decrease in solubility (Figure 2A) suggest the formation of $Cu(DDC)_2$ complex.

XRD Patterns.

Then, the powder XRD patterns of DSF, Cu-Cy, and DSF/Cu-Cy at various ratios (10:1, 1:1, 1:4, 1:8 and 50:1) were collected (Figure 2E). There are two obvious changes in XRD patterns from DSF to DSF/Cu-Cy (10:1). Three new peaks are seen as labeled by the black arrows indicating the formation of new material resulting from the reaction between Cu-Cy and DSF, which can be better visualized in the enlarged view of the XRD patterns of DSF, DSF/Cu-Cy (1:4) and Cu-Cy NPs. On the other hand, other new peaks in the XRD patterns of 10:1 display the residue DSF forms a different crystal structure attributed to the reaction condition. The further increase of Cu-Cy between DSF to Cu-Cy to 1:1, 1:4 and 1:8 results

in the noticeable peaks of Cu-Cy, while the three new peaks seen in the DSF/Cu-Cy (10:1) were diminished and completely disappeared in DSF/Cu-Cy (1:8).

Fourier-Transform Infrared Spectroscopy (FTIR) Analysis.

Finally, the FTIR spectra of DSF+Cu-Cy (DSF:Cu-Cy=1:4), DSF, and Cu-Cy powders were compared (Figure 2F). In the FTIR spectrum of DSF+Cu-Cy (DSF:Cu-Cy=1:4), all the characteristic peaks of Cu-Cy NPs were present, with the reduction in the intensity peaks of Cu-Cy as compared to bare Cu-Cy results suggesting that DSF reacted with Cu-Cy. The characteristic absorption peak at 997 cm^{-1} can be assigned to the stretching vibrations C-S and the ν(C-S) value indicates that the sulfur in the diethyldithiocarbamate coordinated with the metal cation[31–32]. These results further suggest that DSF reacted with Cu-Cy, and a new material was formed, which is consistent with all the results as described above.

DSF and Cu-Cy at Ratio 1:4 Presented the Best Effect to Inhibit Cell Proliferation and Induce Apoptosis in KYSE-30 cells.

The anti-cancer effect of the combination of DSF and Cu-Cy at various ratios was tested in KYSE-30 cells. As a copper(II) donor, $CuCl_2$ was included as a positive control. Since one molecule of Cu-Cy contains three atoms of copper, the concentration of $CuCl_2$ in the control group was 12 μM. As shown in Figure 3A, DSF/Cu-Cy (in μM, 1:4) achieved the lowest cell viability (3%), which presented a slightly better inhibitory effect than DSF/Cu-Cy (1:8) group and the same effect as $CuCl_2$ control group. Data suggest that the nanostructure of Cu-Cy does not interfere with the reaction between copper and DSF. The nucleus staining images of Hoesct dye 33342 revealed condensed chromatin (arrow heads) and loss of nuclei membrane integrity in KYSE-30 cells treated with DSF+Cu-Cy NPs and DSF+$CuCl_2$, which were absent in control, DSF only, or Cu-Cy only groups (Figure 3B). Data suggest that DSF +Cu-Cy NPs could induce cell apoptosis and have a greatly enhanced anti-cancer effect on EC cells.

DSF and Cu-Cy NPs Produced ROS.

To reveal the mechanism underlying the enhanced anti-cancer effect of DSF+Cu-Cy NPs, the production of ROS was examined. A nonfluorescent probe DHR was used in aqueous solution. It is known to react with ROS leading to the formation of a fluorescent molecule, rhodamine 123[22]. The relative PL intensity at 524 nm enhanced significantly after using DSF+Cu-Cy+H_2O_2 as compared to DI water alone, DSF alone, H_2O_2 alone, or DSF+H_2O_2, revealing that the combination of Cu-Cy and DSF can produce ROS (Figure 4A). For comparison, the ROS generation ability of Cu-Cy+H_2O_2 was also measured. It is worthwhile to note that Cu-Cy+H_2O_2 produced more ROS as compared to DSF+Cu-Cy+H_2O_2, which can be attributed to the scavenging role of DSF. The relative PL intensities were lesser after using DSF alone as compared to DI water alone; H_2O_2+DSF as compared to H_2O_2 alone, which demonstrates that DSF is a scavenger of ROS as discussed in the literature[25].

Cu-Cy NPs have been shown to be able to generate •OH through Fenton-like reaction[20]. We next measured the production of •OH using coumarin as a •OH trapping agent. When coumarin reacts with •OH, it produces 7-hydroxycoumarin, a highly fluorescent molecule[33–35]. The relative intensity of 7-hydroxycoumarin at 452 nm enhanced

significantly in H_2O_2 alone, indicating •OH production. DSF+H_2O_2 showed apparent loss in •OH production, confirming, again, DSF as an antioxidant (Figure 4B). In the presence of DSF+Cu-Cy +H_2O_2, the relative PL intensity of 7-hydroxycoumarin at 452 nm enhanced significantly when compared to DI water alone or DSF+H_2O_2 or H_2O_2 alone, justifying the higher amount of •OH production (Figure 4B). However, •OH produced by Cu-Cy+DSF +H_2O_2 was less when compared to Cu-Cy+H_2O_2, again, which could be due to the ROS scavenging capability of DSF[25] and is consistent with the results of detection of ROS using the DHR probe (Figure 4A). Intracellular ROS was further examined in KYSE-30 cells loaded with ROS fluorescent probe DHE. Intracellular DHE fluorescence increased gradually after treatment, especially with Cu-Cy NPs (1μM) or Cu-Cy (1μM) + DSF (4μM) (Figure 4C). However, there was no statistical significance between any two of these groups, implying ROS accumulation may not be the major cause for cell death in cells treated with Cu-Cy NPs and DSF.

Combination of CuCy and DSF Inhibited Nuclear Translocation of NF-κB (p65).

Next, cellular mechanism and signaling pathways were examined in cancer cells upon the treatment of DSF+Cu-Cy NPs. NF-κB (p65) is a major transcription factor in cell proliferation. Nuclear translocation of p65 was compared among groups of DSF+Cu-Cy NPs, DSF+$CuCl_2$, DSF only, Cu-Cy only and control. After starvation and drug incubation for 2 h, KYSE-30 cells were stimulated with 10% FBS to induce the translocation of NF-κB (p65) from cytosol to the nucleus (Protocol illustrated in Figure 5A). In the control or single-agent treated groups, there were 13–14% cells with NF-κB (p65) located in the nucleus. But in DSF+Cu-Cy group, the cell number with NF-κB (p65) nuclear localization was decreased to 1.4 %, similar to DSF+$CuCl_2$ group (Figure 5B). The results demonstrated that a combination of DSF and Cu-Cy NPs inhibited NF-κB (p65) signaling pathways in KYSE-30 cells.

Combination of DSF and Cu-Cy NPs Inhibited Tumor Growth in Xenograft EC Mice.

The *in vivo* anti-cancer effect of Cu-Cy NPs and DSF was tested in xenograft nude mice bearing KYSE-30 cells. After inoculation, the mice were divided into five groups with the treatment of vehicle control, 1 μM of DSF alone, 4 μM of Cu-Cy alone, 1 μM of DSF and 4 μM of Cu-Cy, 1 μM of DSF and 12 μM of $CuCl_2$. In each group, the body weight and tumor volume were measured every two days (Figure 6A–B). In statistical analysis, the tumor volume was first log2 transformed to reduce variance and skewness. A linear mixed effects model was introduced to take account of the correlation among observations from the same animal. The results showed that treatment of combined DSF+Cu-Cy significantly decreased tumor volume compared to control and single agent groups averaged over time between days 20 and 46 without correction for multiple comparisons. It was considered that the time taken by agents to present effect and the tumor growth were similar before day 20. There was significant difference in the trend of tumor growth over time between DSF+Cu-Cy and DSF group (p-value=0.0008), but not between other groups, which had similar growth rate. It is noteworthy that no significant differences were observed in body weight among all treatment groups except in DSF+$CuCl_2$ group. Mice in DSF+$CuCl_2$ group presented almost 20% body weight lost after 10 days of treatment. Treatment had to be terminated in this group following animal welfare recommendation. At day 32, animals were euthanized. Tumor

tissue, heart, liver, spleen, kidney, and lung of each animal were collected and subject to H&E staining. The H&E images revealed normal tissue histology in heart, kidney, spleen, liver, and lung in the groups of vehicle control, Cu-Cy, DSF, and DSF+Cu-Cy. In DSF +$CuCl_2$ treated animals, however, there were signs of tissue damage in the heart, kidney, spleen, and liver (Figure 6C). The tissue toxicity data was consistent with the observation of significant body weight loss in these animals.

DISCUSSION

In this contribution, the anti-cancer effect of the combination of DSF and Cu-Cy NPs was evaluated in cultured ESCC cells and in vivo. Data showed that Cu-Cy NPs could greatly facilitate DSF to inhibit cell proliferation and induce apoptosis. Interestingly, the combined inhibitory function could be even further enhanced when DSF and Cu-Cy NPs presented an optimal molar ratio of 1:4. The change in physical color and the spectra of UV-vis absorption, XRD patterns, and FTIR spectra from mixtures of DSF and Cu-Cy NPs suggest the formation of new materials The mechanistic studies revealed that combination of DSF and Cu-Cy NPs blocked the nuclear translocation of NF-ƙB (p65) in ESCC cells.

We also demonstrated that the combined administration of DSF and Cu-Cy greatly inhibited tumor growth without noticeable histological toxicity in xenograft nude mice. Together, this study demonstrates the effective anti-cancer function of combined treatment of DSF and Cu-Cy NPs *in vitro* and *in vivo*, which could be a promising new chemotherapy for esophageal cancer patients.

Consistent with previous reports, we found that the full anti-cancer effect of DSF requires adjuvant Cu^{2+} ions, which can be supplied either through $CuCl_2$ or Cu-Cy NPs. In many clinical studies, Cu^{2+} ions (such as in Cu gluconate) are delivered orally or through intravenous injection, thereby increasing levels of Cu^{2+} ions in the body. Due to its toxicity as a heavy metal and short systemic half-life, Cu^{2+} concentration may not easily reach a therapeutic window to work together with DSF in the human body[6]. Consequently, the administration of preformed $Cu(DDC)_2$ in a single formulation has become to be a more effective strategy to acquire a higher $Cu(DDC)_2$ amount in tumors with increased anti-cancer efficacy[24, 26]. However, the poor aqueous solubility of the $Cu(DDC)_2$ hampers its clinical use. In this work, both *in vitro* and *in vivo* data showed that Cu-Cy NPs were able to provide Cu^{2+} ions to react with DSF in cancer cells. The results of the change in physical color, the UV-vis absorption and fluorescence spectra, XRD patterns, and FTIR spectra all suggest that Cu-Cy NPs reacted with DSF and formed new materials, such as $Cu(DDC)_2$ (Figure 2). The formation of $Cu(DDC)_2$ was best demonstrated by the absorption peak at about 433 nm, which is the signature peak of $Cu(DDC)_2$ (Figure 2C–D). It is well known that NPs can be either passively accumulated into tumors via EPR effect or selectively targeted to tumors via cancer specific markers. Therefore, Cu-Cy NPs may have even more advantages than Cu gluconate to reach high enough concentration in tumor but less in normal tissues to work together with DSF. Additionally, Cu-Cy NPs have good solubility in blood stream, reduced potential immunogenicity, and stabilized and prolonged half-life. These advantages make Cu-Cy a better copper provider to assist DSF and largely reduces the toxicity to cells and animals. Furthermore, Cu-Cy NPs can serve as photosensitizers used in different

radiotherapies, from UV light to X-ray, from microwave to ultrasound based cancer treatment[11–14, 16, 19, 21]. Therefore, Cu-Cy NPs + DSF may not only be effective chemotherapy by itself, but also provide a possible adjuvant therapy with radiotherapy or phototherapy.

Another important finding of this work is the identification of the optimal ratio between DSF and Cu^{2+} in anti-cancer function. This study showed that the molar ratio of DSF and Cu-Cy was optimized to 1:4 (Figure 3A), which made the ratio of DSF and Cu^{2+} was 1:12 (each molecule of Cu-Cy contained 3 atoms of Cu). This result is very similar like the molar ratio range of DSF to Cu^{2+} (i.e. 1:6) used in the treatment of melanoma in a previous report[30]. These data are consistent to suggest that the new complex material formed by DSF and Cu may be the key contributor to the anti-tumor effect.

It has been reported that DSF/Cu targets cancer cells by the combination of two actions: (1) instant cell death caused by the production of ROS as a result of the reaction between DSF and Cu, and (2) delayed cell killing introduced by the toxic nature of the end product, DSF-Cu complex[36]. To evaluate whether ROS accumulation plays a role in DSF/Cu-Cy NPs mediated anti-cancer function, we measured ROS, including •OH, in cell-free system and in cultured ESCC cells. Cu-Cy NPs alone had the best capability to produce ROS, including •OH, and DSF acted as a ROS scavenger with reduced ROS and •OH (Figure 4). Since DSF +Cu-Cy NPs had a better anti-cancer effect even with less production of ROS, including •OH, than Cu-Cy alone, these results indicate that generation of ROS, including •OH, may not be the key mechanism underlying the anti-cancer effect of DSF/Cu-Cy.

The anti-cancer effect of DSF and Cu-Cy relied on not only inhibiting cell proliferation but also on the induction of apoptosis (Figure 3). Several transcription factors have been demonstrated to play a key role in cell proliferation and apoptosis in ESCC. NF-κB is one of them[37]. This transcription factor family contains p65/RelA, p50, p52, c-Rel, and RelB. When activated, IκB complex releases NF-κB (p65) which translocates from cytosol to nucleus[38]. As shown Figure 5, DSF+Cu-Cy NPs clearly blocked nuclear translocation of NF-κB in KYSE-30 cells. Since NF-κB signaling pathway is also known to be involved in epithelial–mesenchymal transition and metastasis, the administration of DSF+Cu-Cy NPs could be beneficial for metastatic ESCC cases too. Combination of DSF and Cu has been shown to decrease drug resistance of chemotherapy drug in both colon and breast cancer[39], it will be of importance to investigate whether DSF+Cu-Cy NPs could overcome drug resistance in ESCC cells in the future.

CONCLUSIONS

This study provided evidence to show that Cu-Cy NP is a new and safer agent providing Cu to work together with DSF to significantly improve the anti-cancer effect in esophageal cancer. The enhanced cytotoxic nature of Cu-Cy+DSF may be ascribed to the synergetic effect of the ROS production and formation of DSF-Cu complex. The formation of the DSF-Cu complex can be supported by the evidence of change in the physical color, fluorescence and absorption spectra, XRD patterns, and FTIR spectra. Data further showed that the combination of DSF and Cu-Cy induced cell apoptosis, and blocked the translocation of NF-

ĸB (p65) into the nucleus in ESCC cells. This work may provide some insight to pave the way for the development of a new chemotherapy strategy using DSF and CuCy NPs for EC and other cancer patients. Further investigation on how to improve the stability of DSF and CuCy NPs in the bloodstream and how to combine with other treatments, such as radiotherapy and photodynamic therapy, are warranted.

Acknowledgments

This work was supported by U.S. National Institutes of Health (NIH) Grant R01 CA185055 and S10 OD025230 (to ZP). We would like to acknowledge the distinguished award from the University of Texas at Arlington as well as support from Solgro Inc. We thank Dr. Roy McDougald for helping with FTIR measurement.

REFERENCES

(1). Cui C; Chang Y; Zhang X; Choi S; Tran H; Penmetsa KV; Viswanadha S; Fu L; Pan Z Targeting Orai1-mediated store-operated calcium entry by RP4010 for anti-tumor activity in esophagus squamous cell carcinoma. Cancer letters 2018, DOI: 10.1016/j.canlet.2018.06.006.

(2). Skrott Z; Mistrik M; Andersen KK; Friis S; Majera D; Gursky J; Ozdian T; Bartkova J; Turi Z; Moudry P; Kraus M; Michalova M; Vaclavkova J; Dzubak P; Vrobel I; Pouckova P; Sedlacek J; Miklovicova A; Kutt A; Li J; Mattova J; Driessen C; Dou QP; Olsen J; Hajduch M; Cvek B; Deshaies RJ; Bartek J Alcohol-abuse drug disulfiram targets cancer via p97 segregase adaptor NPL4. Nature 2017, 552 (7684), 194–199, DOI: 10.1038/nature25016. [PubMed: 29211715]

(3). Sleire L; Forde HE; Netland IA; Leiss L; Skeie BS; Enger PO Drug repurposing in cancer. Pharmacol Res 2017, 124, 74–91, DOI: 10.1016/j.phrs.2017.07.013. [PubMed: 28712971]

(4). Wright C; Moore RD Disulfiram treatment of alcoholism. The American journal of medicine 1990, 88 (6), 647–55, DOI: 10.1016/0002-9343(90)90534-k. [PubMed: 2189310]

(5). Suh JJ; Pettinati HM; Kampman KM; O'Brien CP The status of disulfiram: a half of a century later. J Clin Psychopharmacol 2006, 26 (3), 290–302, DOI: 10.1097/01.jcp.0000222512.25649.08. [PubMed: 16702894]

(6). McMahon A; Chen W; Li F Old wine in new bottles: Advanced drug delivery systems for disulfiram-based cancer therapy. J Control Release 2020, 319, 352–359, DOI: 10.1016/j.jconrel.2020.01.001. [PubMed: 31911155]

(7). Li H; Wang J; Wu C; Wang L; Chen ZS; Cui W The combination of disulfiram and copper for cancer treatment. Drug discovery today 2020, DOI: 10.1016/j.drudis.2020.04.003.

(8). Chen D; Cui QZC; Yang HJ; Dou QP Disulfiram, a clinically used anti-alcoholism drug and copper-binding agent, induces apoptotic cell death in breast cancer cultures and xenografts via inhibition of the proteasome activity. Cancer research 2006, 66 (21), 10425–10433, DOI: 10.1158/0008-5472.Can-06-2126. [PubMed: 17079463]

(9). Gupte A; Mumper RJ Elevated copper and oxidative stress in cancer cells as a target for cancer treatment. Cancer treatment reviews 2009, 35 (1), 32–46, DOI: 10.1016/j.ctrv.2008.07.004. [PubMed: 18774652]

(10). Fan Z; Chang Y; Cui C; Sun L; Wang DH; Pan Z; Zhang M Near infrared fluorescent peptide nanoparticles for enhancing esophageal cancer therapeutic efficacy. Nature communications 2018, 9 (1), 2605, DOI: 10.1038/s41467-018-04763-y.

(11). Pandey NK; Chudal L; Phan J; Lin L; Johnson O; Xing M; Liu P; Li H; Huang X; Shu Y; Chen W A facile method for synthesis of copper-cysteamine nanoparticles and study of ROS production for cancer treatment. J. Mater. Chem. B 2019, 7, 6630–6642. [PubMed: 31591609]

(12). Ma L; Zou X; Chen W A new X-ray activated nanoparticle photosensitizer for cancer treatment. Journal of biomedical nanotechnology 2014, 10 (8), 1501–8, DOI: 10.1166/jbn.2014.1954. [PubMed: 25016650]

(13). Shrestha S; Wu J; Sah B; Vanasse A; Cooper LN; Ma L; Li G; Zheng H; Chen W; Antosh MP X-ray induced photodynamic therapy with copper-cysteamine nanoparticles in mice tumors.

Proceedings of the National Academy of Sciences of the United States of America 2019, 116 (34), 16823–16828, DOI: 10.1073/pnas.1900502116. [PubMed: 31371494]

(14). Liu Z; Xiong L; Ouyang G; Ma L; Sahi S; Wang K; Lin L; Huang H; Miao X; Chen W; Wen Y Investigation of Copper Cysteamine Nanoparticles as a New Type of Radiosensitiers for Colorectal Carcinoma Treatment. Scientific reports 2017, 7 (1), 9290, DOI: 10.1038/s41598-017-09375-y. [PubMed: 28839163]

(15). Sah B; Wu J; Vanasse A; Pandey NK; Chudal L; Huang Z; Song W; Yu H; Ma L; Chen W; Antosh MP Effects of Nanoparticle Size and Radiation Energy on Copper-Cysteamine Nanoparticles for X-ray Induced Photodynamic Therapy. Nanomaterials 2020, 10 (6), DOI: 10.3390/nano10061087.

(16). Yao M; Ma L; Li L; Zhang J; Lim RX; Chen W; Zhang Y A New Modality for Cancer Treatment—Nanoparticle Mediated Microwave Induced Photodynamic Therapy. J. Biomed. Nanotechnol 2016, 12, 1835–1851. [PubMed: 29359896]

(17). Zhang Q; Guo XD; Cheng YN; Chudal L; Pandey NK; Zhang JY; Ma L; Xi Q; Yang GZ; Chen Y; Ran X; Wang CZ; Zhao JY; Li Y; Liu L; Yao Z; Chen W; Ran YP; Zhang RX Use of copper-cysteamine nanoparticles to simultaneously enable radiotherapy, oxidative therapy and immunotherapy for melanoma treatment. Signal Transduct Tar 2020, 5 (1), DOI: 10.1038/s41392-020-0156-4.

(18). Zhen X; Chudal L; Pandey NK; Phan J; Ran X; Amador E; Huang X; Johnson O; Ran Y; Chen W; Hamblin MR; Huang L A powerful combination of copper-cysteamine nanoparticles with potassium iodide for bacterial destruction. Materials science & engineering. C, Materials for biological applications 2020, 110, 110659, DOI: 10.1016/j.msec.2020.110659. [PubMed: 32204087]

(19). Wang P; Wang X; Ma L; Sahi S; Li L; Wang X; Wang Q; Chen Y; Chen W; Liu Q Nanosonosensitization by Using Copper-Cysteamine Nanoparticles Augmented Sonodynamic Cancer Treatment. Part Part Syst Char 2018, 35 (4), 1700378, DOI: 10.1002/ppsc.201700378.

(20). Chudal L; Pandey NK; Phan J; Johnson O; Lin L; Yu H; Shu Y; Huang Z; Xing M; Liu JP; Chen M-L; Chen W Copper-cysteamine Nanoparticles as a Heterogeneous Fenton-like Catalyst for Highly Selective Cancer Treatment ACS Applied Biomaterials 2020, 3 (3), 1804–1814.

(21). Ma L; Chen W; Schatte G; Wang W; Joly AG; Huang Y; Sammynaiken R; Hossu M A new Cu–cysteamine complex: structure and optical properties. J. Mater. Chem. C 2014, 2 (21), 4239–4246, DOI: 10.1039/c4tc00114a.

(22). Gomes A; Fernandes E; Lima JL Fluorescence probes used for detection of reactive oxygen species. J Biochem Bioph Meth 2005, 65 (2–3), 45–80, DOI: 10.1016/j.jbbm.2005.10.003.

(23). Zhu H; Zhang H; Jin F; Fang M; Huang M; Yang CS; Chen T; Fu L; Pan Z Elevated Orai1 expression mediates tumor-promoting intracellular Ca2+ oscillations in human esophageal squamous cell carcinoma. Oncotarget 2014, 5 (11), 3455–71, DOI: 10.18632/oncotarget.1903. [PubMed: 24797725]

(24). Wehbe M; Anantha M; Backstrom I; Leung A; Chen K; Malhotra A; Edwards K; Bally MB Nanoscale Reaction Vessels Designed for Synthesis of Copper-Drug Complexes Suitable for Preclinical Development. PloS one 2016, 11 (4), e0153416, DOI: 10.1371/journal.pone.0153416. [PubMed: 27055237]

(25). Orrenius S; Nobel C; Van den Dobbelsteen D; Burkitt M; Slater A, Dithiocarbamates and the redox regulation of cell death. Portland Press Ltd.: 1996.

(26). Wu W; Yu L; Jiang Q; Huo M; Lin H; Wang L; Chen Y; Shi J Enhanced Tumor-Specific Disulfiram Chemotherapy by In Situ Cu(2+) Chelation-Initiated Nontoxicity-to-Toxicity Transition. J Am Chem Soc 2019, 141 (29), 11531–11539, DOI: 10.1021/jacs.9b03503. [PubMed: 31251050]

(27). Lewis DJ; Deshmukh P; Tedstone AA; Tuna F; O'Brien P On the interaction of copper(II) with disulfiram. Chem Commun (Camb) 2014, 50 (87), 13334–7, DOI: 10.1039/c4cc04767b. [PubMed: 25233190]

(28). Plyusnin VF; Kolomeets AV; Grivin VP; Larionov SV; Lemmetyinen H Photochemistry of dithiocarbamate Cu(II) complex in CCl4. J Phys Chem A 2011, 115 (10), 1763–73, DOI: 10.1021/jp105755f. [PubMed: 21341781]

(29). Chang Y; Jiang J; Chen W; Yang W; Chen L; Chen P; Shen J; Qian S; Zhou T; Wu L Biomimetic metal-organic nanoparticles prepared with a 3D-printed microfluidic device as a novel formulation for disulfiram-based therapy against breast cancer. Applied Materials Today 2020, 18, 100492.

(30). Cen D; Brayton D; Shahandeh B; Meyskens FL Jr.; Farmer PJ Disulfiram facilitates intracellular Cu uptake and induces apoptosis in human melanoma cells. J Med Chem 2004, 47 (27), 6914–20, DOI: 10.1021/jm049568z. [PubMed: 15615540]

(31). Siadatnasab F; Farhadi S; Dusek M; Eigner V; Hoseini A-A; Khataee A Sonochemical synthesis and structural characterization of an organic-inorganic nanohybrid based on a copper-dithiocarbamate complex and PMo12O403− polyanion as a novel sonocatalyst. Ultrason. Sonochem 2019, 104727. [PubMed: 31810872]

(32). Farhadi S; Siadatnasab F Copper (I) sulfide (Cu2S) nanoparticles from Cu (II) diethyldithiocarbamate: synthesis, characterization and its application in ultrasound-assisted catalytic degradation of organic dye pollutants. Mater. Res. Bull 2016, 83, 345–353.

(33). Louit G; Foley S; Cabillic J; Coffigny H; Taran F; Valleix A; Renault JP; Pin S The reaction of coumarin with the OH radical revisited: hydroxylation product analysis determined by fluorescence and chromatography. Radiat Phys Chem 2005, 72 (2–3), 119–124, DOI: 10.1016/j.radphyschem.2004.09.007.

(34). Czili H; Horváth A Applicability of coumarin for detecting and measuring hydroxyl radicals generated by photoexcitation of TiO2 nanoparticles. Appl Catal B-Environ 2008, 81 (3–4), 295–302, DOI: 10.1016/j.apcatb.2008.01.001.

(35). Nosaka Y; Nosaka AY Generation and Detection of Reactive Oxygen Species in Photocatalysis. Chem Rev 2017, 117 (17), 11302–11336, DOI: 10.1021/acs.chemrev.7b00161. [PubMed: 28777548]

(36). Tawari PE; Wang Z; Najlah M; Tsang CW; Kannappan V; Liu P; McConville C; He B; Armesilla AL; Wang W The cytotoxic mechanisms of disulfiram and copper(ii) in cancer cells. Toxicology research 2015, 4 (6), 1439–1442, DOI: 10.1039/c5tx00210a. [PubMed: 27708770]

(37). Chapman NR; Webster GA; Gillespie PJ; Wilson BJ; Crouch DH; Perkins ND A novel form of the RelA nuclear factor kappaB subunit is induced by and forms a complex with the proto-oncogene c-Myc. The Biochemical journal 2002, 366 (Pt 2), 459–69, DOI: 10.1042/BJ20020444. [PubMed: 12027803]

(38). Baeuerle PA; Baltimore D NF-kappa B: ten years after. Cell 1996, 87 (1), 13–20. [PubMed: 8858144]

(39). Guo X; Xu B; Pandey S; Goessl E; Brown J; Armesilla AL; Darling JL; Wang W Disulfiram/copper complex inhibiting NFkappaB activity and potentiating cytotoxic effect of gemcitabine on colon and breast cancer cell lines. Cancer letters 2010, 290 (1), 104–13, DOI: 10.1016/j.canlet.2009.09.002. [PubMed: 19782464]

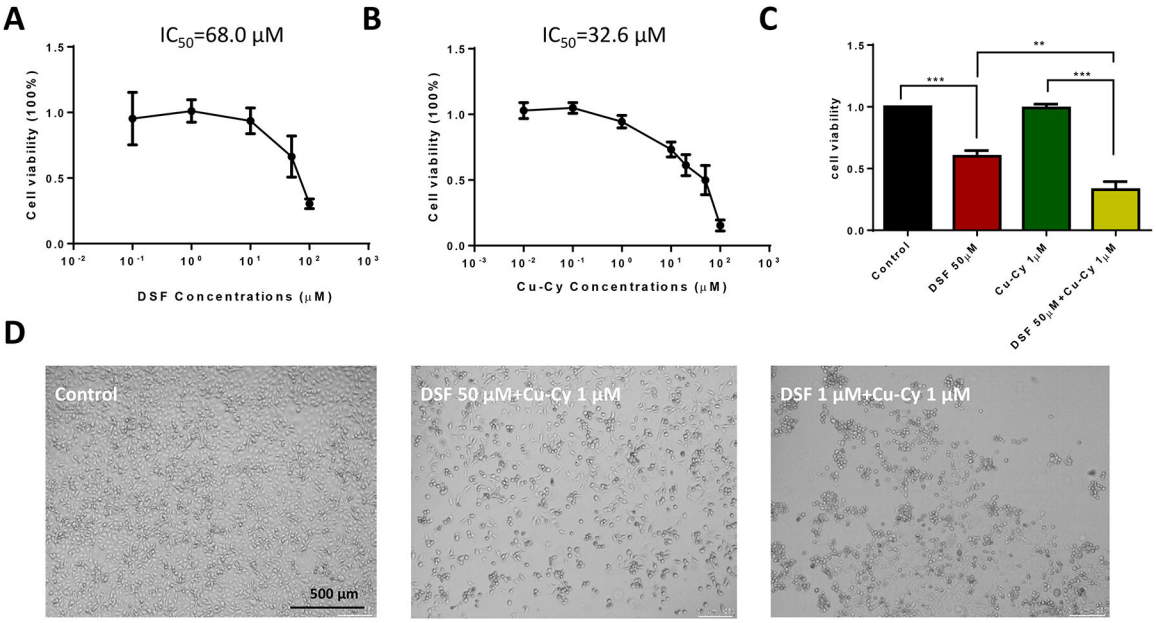

Figure 1.

Combination of disulfiram (DSF) and Cu-Cy nanoparticles (NPs) inhibiting cell proliferation in KYSE-30 cells. **A**. Dose-dependent curve of DSF in cell viability. **B**. Dose-dependent curve of Cu-Cy NPs in cell viability. **C**. Statistics of cell viability among the different groups. Data are shown as mean ± S.E.M., ** $p \leq 0.01$, *** $p \leq 0.001$, n=3. **D**. Phase contrast images of KYSE-30 cells treated with vehicle only (control), DSF combined with Cu-Cy NPs (1 μM) at either 50 μM or 1 μM. Note, DSF at 1 μM induced more cell death than at 50 μM with 1 μM Cu-Cy NPs.

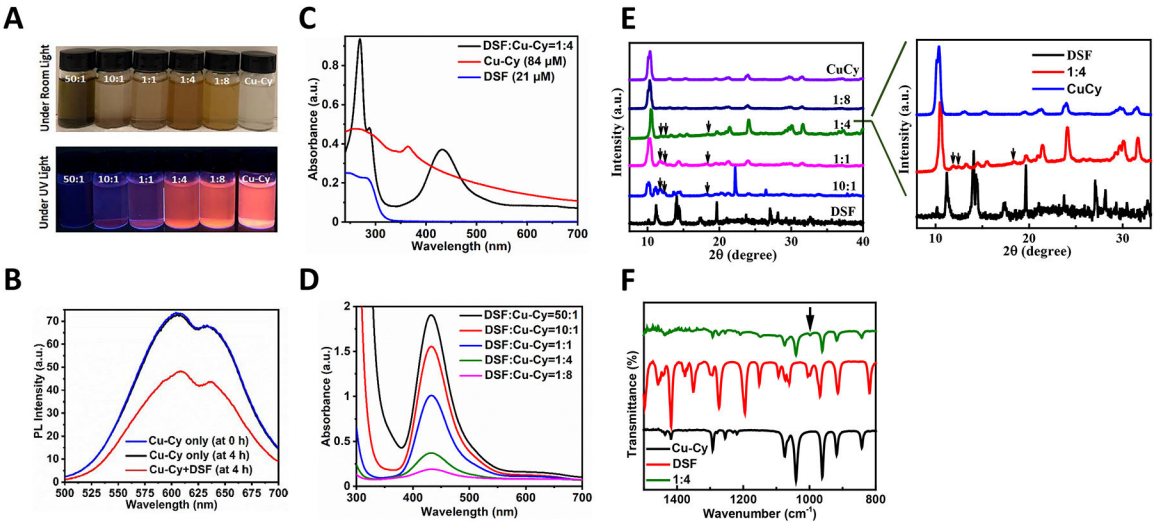

Figure 2.

Formation of new material in a mixture of DSF and Cu-Cy NPs. **A**. Pictures of the various ratios of DSF to Cu-Cy NPs (DSF: Cu-Cy=50:1, 10:1, 1:1, 1:4, and 1:8) and Cu-Cy NPs alone (from left to right) after 4 h of incubation upon room light (top) and ultraviolet (UV) light (bottom). **B**. Photoluminescence (PL) spectra of Cu-Cy NPs and Cu-Cy+DSF (DSF:Cu-Cy=1:4) with the excitation wavelength of 365 nm. **C**. UV-vis absorption spectra of DSF:Cu-Cy at 1:4, Cu-Cy (84 μM), and DSF (21 μM) dispersed in ethanol. **D**. UV-vis absorption spectra of various molar ratios of DSF to Cu-Cy (50:1, 10:1, 1:1, 1:4, and 1:8, respectively) dispersed in ethanol. **E**. X-ray diffraction (XRD) patterns of Cu-Cy NPs mixed with DSF at various ratios (DSF: Cu-Cy at 10:1, 1:1, 1:4 and 1:8), Cu-Cy alone and DSF alone. Inserted panel is an enlarged view of the XRD spectra of Cu-Cy NPs mixed with disulfiram (DSF:Cu-Cy at 1:4). Three black arrows indicate the new peaks observed. **F**. Fourier-transform infrared (FTIR) spectra of DSF:Cu-Cy=1:4, DSF, and Cu-Cy powders. The black arrow indicates the characteristic absorption peak at 997 cm^{-1}.

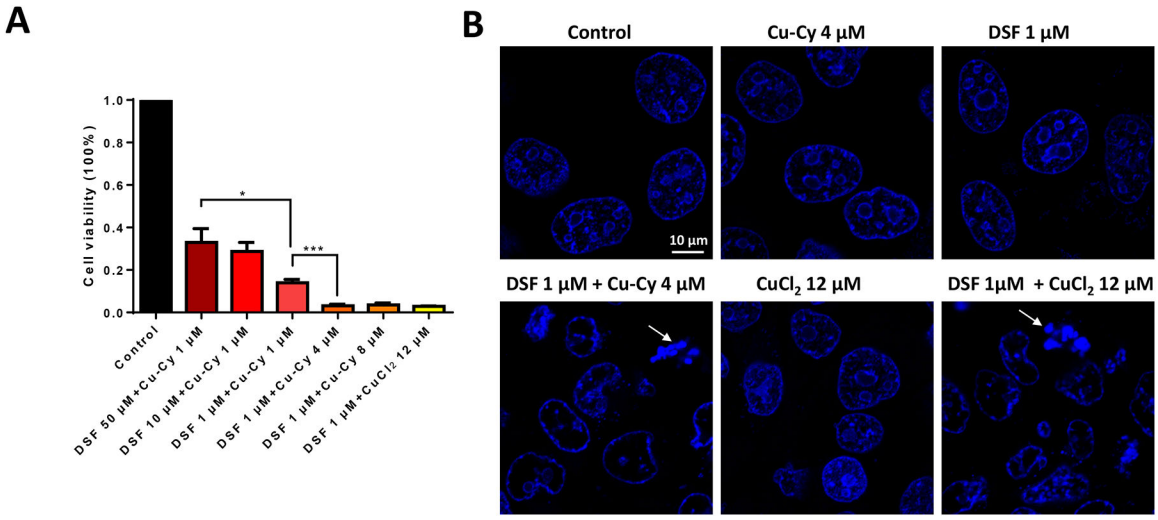

Figure 3.

Reduced cell viability in KYSE-30 cells treated with DSF and Cu-Cy NPs at various ratio. **A**. Cell viability of KYSE-30 cells treated with DSF, Cu-Cy NPs or combination at various ratio as indicated. Cell numbers are normalized with cells cultured in normal growth medium without any addition (control). Data are represented as the mean ± S.E.M, * $p \leq 0.05$, ** $p \leq 0.01$, n=3. **B**. Confocal microscopy images of nuclei with hoechst staining. Cells were treated with DSF, Cu-Cy NPs or combination. Arrows point out nuclear fragmentation and condensation, a hall mark of apoptosis. Scale bar, 10 μm.

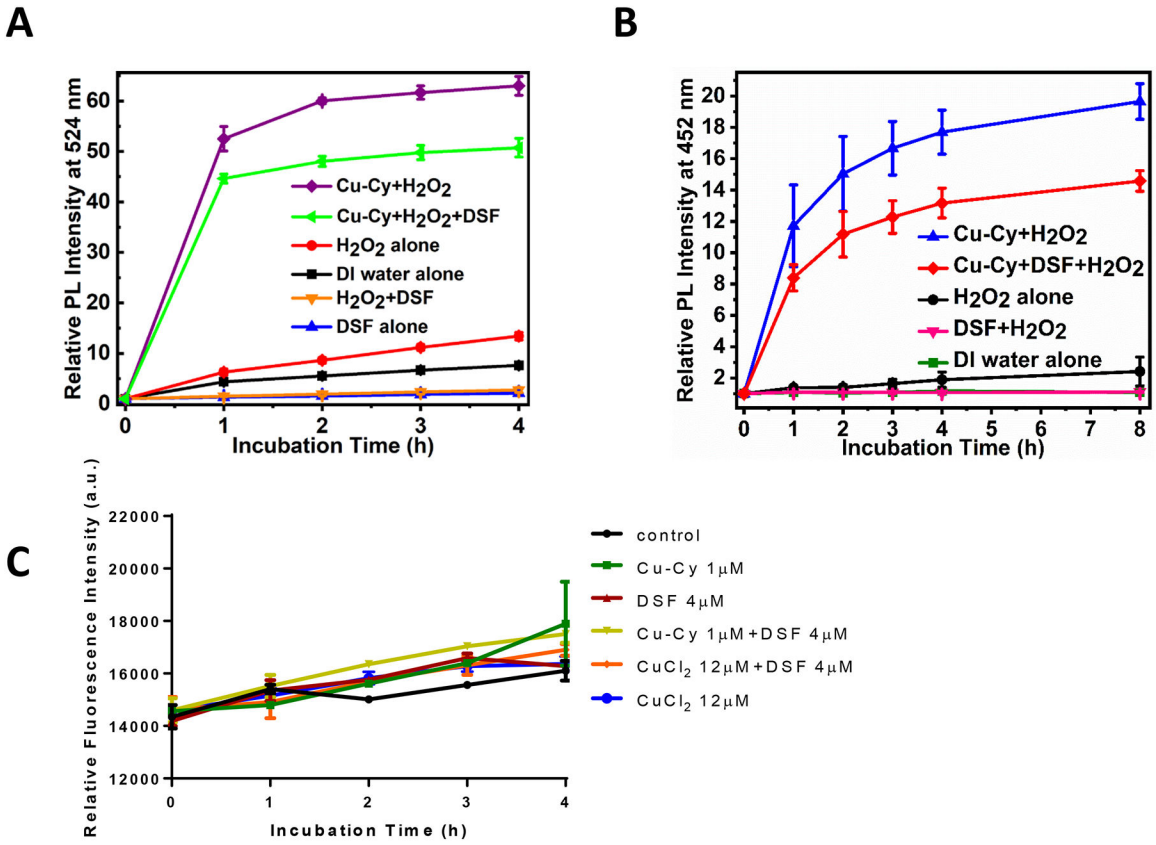

Figure 4.

Detection of ROS and hydroxyl radical (•OH) production in solutions containing Cu-Cy NPs using fluorescent probes. **A.** Relationship between the relative photoluminescence (PL) intensity at 524 nm with incubation time. The enhancement in the relative PL intensity shows the generation of ROS. The excitation and emission wavelengths were 495 nm and 524 nm, respectively. **B.** Relationship between the relative photoluminescence (PL) intensity at 452 nm with incubation time. The enhancement in the relative PL intensity shows the generation of hydroxyl radical (•OH). The excitation and emission wavelengths were 332 nm and 452 nm, respectively. The data are presented as the mean ± standard deviation from the three independent experiments. **C**. Intracellular ROS measurement using fluorescent probe DHE. DHE fluorescence was measured in KYSE-30 cells treated with Cu-Cy (1 μM), DSF (4 μM), Cu-Cy (1 μM)+DSF (4 μM), $CuCl_2$ (12 μM), $CuCl_2$ (12 μM)+DSF (4 μM) for indicated hours. The data are shown as the mean ± S.E.M., n=18 from 2 independent biological replicates.

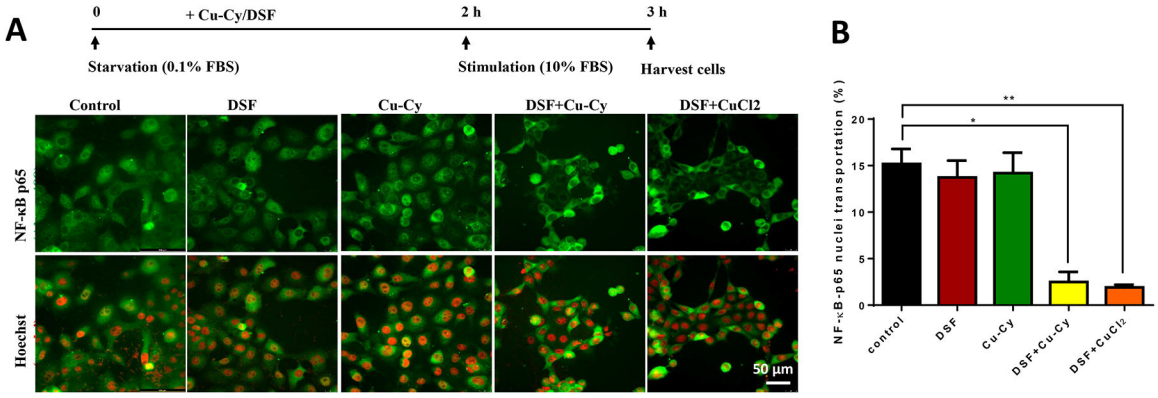

Figure 5.

Combined treatment of Cu-Cy and DSF inhibiting NF-ƙB (p65) nuclear translocation. **A**. Immunostaining of NF-ƘB (p65) (green) and Hoechst nuclei (red) in KYSE-30 cells. The treatment protocol is shown at the top. Cells were starved in 0.1% FBS for 2 hours and then switched to 10% FBS to initiate stimulation. NF-ƙB (p65) is stained with antibody (green) and nuclei is stained with Hoechst (red). Scale bar, 50 μm. **B**. The percentage of cells with NF-ƘB (p65) nuclear pattern in each group is calculated. Data are presented as mean ± S.E.M., * $p \leq 0.05$, ** $p \leq 0.01$, n=7.

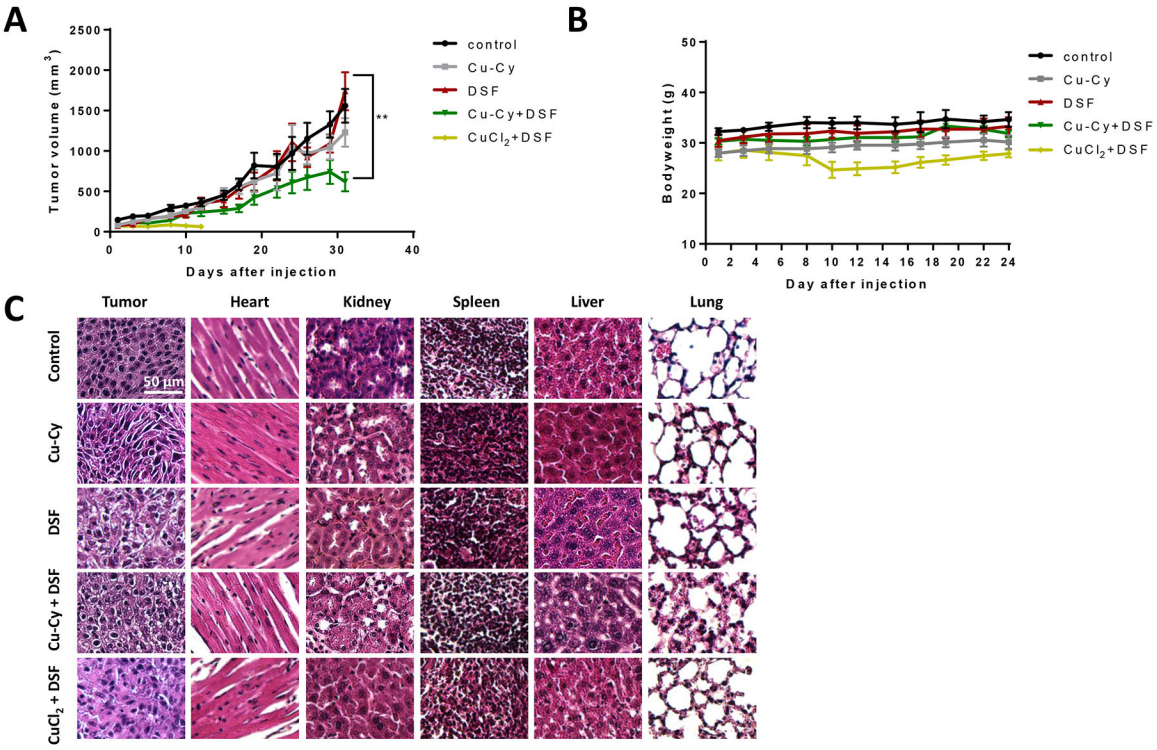

Figure 6.

Combined treatment of Cu-Cy and DSF inhibiting tumor growth in xenograft mice. **A**. Tumor growth curve of xenograft mice in control or treatment groups, i.e. Cu-Cy alone, DSF alone, DSF+Cu-Cy, DSF+$CuCl_2$. Data are presented as as mean ± S.E.M., ** $p \leq 0.01$, n=6. **B**. The bodyweight curves of xenograft nude mice in the control group. Data are shown as as mean ± S.E.M., n=6. **C**. H&E staining of tumor tissue, heart, kidney, spleen, liver and lung in control and different treatment groups. * $p \leq 0.01$, ** $p \leq 0.001$, n=6. Scale bar, 100 μm.